REPORT

Heat source recognition sensor mimicking the thermosensation function of human skin

Wenting Sun,[1,7] Pengxiang Zhang,[1,3,7] Xinyi Lin,[1] Yupeng Wang,[1] Shuaihua Wang,[1] Bin Yang,[1] Zijian Zheng,[3,4,5,6,*] and Weishu Liu[1,2,*]

*Correspondence: zijian.zheng@polyu.edu.hk (Z.Z.); liuws@sustech.edu.cn (W.L.)

Received: April 9, 2024; Accepted: June 30, 2024; Published Online: July 2, 2024; https://doi.org/10.1016/j.xinn.2024.100673

GRAPHICAL ABSTRACT

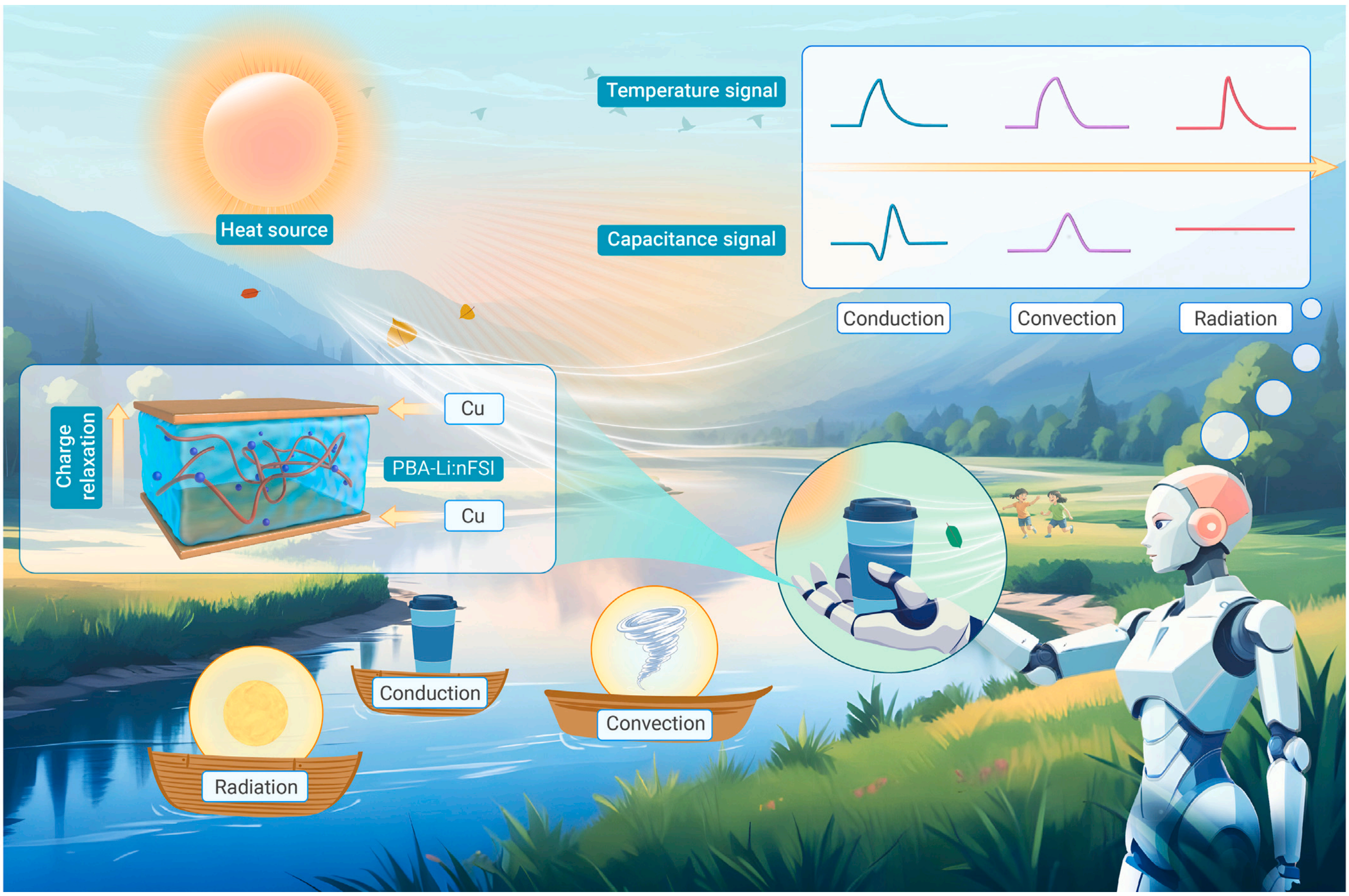

PUBLIC SUMMARY

- The heat source recognition sensor we proposed can simultaneously provide temperature sensing, proximity sensing, and pressure sensing.
- The combined sensing can distinguish the signals of radiation, convection, and conduction.
- Heat source recognizing can provide in-depth temperature sensing information to the robot.

Heat source recognition sensor mimicking the thermosensation function of human skin

Wenting Sun,[1,7] Pengxiang Zhang,[1,3,7] Xinyi Lin,[1] Yupeng Wang,[1] Shuaihua Wang,[1] Bin Yang,[1] Zijian Zheng,[3,4,5,6,*] and Weishu Liu[1,2,*]

[1]Department of Materials Science and Engineering, Southern University and Science and Technology, Shenzhen 518055, China

[2]Guangdong Provincial Key Laboratory of Functional Oxide Materials and Devices, Southern University of Science and Technology, Shenzhen 518055, China

[3]School of Fashion and Textiles, The Hong Kong Polytechnic University, Hong Kong SAR, China

[4]Department of Applied Biology and Chemical Technology, The Hong Kong Polytechnic University, Hong Kong SAR 999077, China

[5]Research Institute for Intelligent Wearable Systems (RI-IWEAR), The Hong Kong Polytechnic University, Hong Kong SAR 999077, China

[6]Research Institute for Smart Energy (RISE), The Hong Kong Polytechnic University, Hong Kong SAR 999077, China

[7]These authors contributed equally

*Correspondence: zijian.zheng@polyu.edu.hk (Z.Z.); liuws@sustech.edu.cn (W.L.)

Received: April 9, 2024; Accepted: June 30, 2024; Published Online: July 2, 2024; https://doi.org/10.1016/j.xinn.2024.100673

Citation: Sun W., Zhang P., Lin X., et al., (2024). Heat source recognition sensor mimicking the thermosensation function of human skin. The Innovation **5(5)**, 100673.

The human skin maintains a comfortable and healthy somatosensory state by sensing different aspects of the thermal environment, including temperature value, heat source, energy level, and duration. However, state-of-the-art thermosensors only measure basic temperature values, not the full range of the thermosensation function of human skin. Here, we propose a heat source recognition (*hsr*) sensor of poly(butyl acrylate)-lithium bis(n-fluoroalkylsulfonyl)imide (PBA-Li:*n*FSI; *n* = 1, 3, 5), which enables response to temperature, pressure, and proximity stimulus signals based on the relaxation behavior of the ionic gel and distinguished between different types of heat sources (i.e., radiation, convection, and conduction). The *hsr* sensor was integrated into a prosthetic limb covered by an e-skin with isothermal regulation, and experiments with a robot showed that it could achieve human-like thermosensation function, recognizing multidimensional information about thermal environments, such as temperature value, comfort level, and heat source signal. This work deeply mimics the human body's thermosensation function and provides a reliable solution for the development of bionic e-skin for intelligent robots and prosthetics.

INTRODUCTION

Thermal functions include thermoregulation and thermosensation, which play critical roles in the physiological and psychological well-being of humans, not only to maintain the healthy life of the human body but also to serve as an important pathway for communication and cognitive learning among individuals.[1] Humans are homeothermic by nature,[1] and heat produced by metabolism and exchanged between the skin and environment is critical to maintaining the thermal balance of the human body. Homeothermy refers to the capability of isothermal regulation.[2,3] Thermoregulation enables humans to maintain an isothermal skin that is sensitive to environmental changes. Our group previously used a flexible thermoelectric device to mimic the isothermoregulation capabilities of the human body and developed an e-skin with isothermal regulation over a wide temperature range for the external environment.[4,5] Just as the mechanical sensing of a variety of stimuli like strain, pressure, and sliding enable the sense of tactile sensation,[6-8] thermosensation involves not only sensing the degree of heat and cold of the external environment but also recognizing information such as the heat source type and duration.[9,10] This multidimensional perception forms a thermosensory sensation system that guarantees that the human being will seek a comfortable environment to make the organism healthy.[11,12] The development of artificial limbs with the full range of thermosensation capabilities will help prosthesis users reconnect with the world and allow intelligent robots to adapt to diverse environments.[13,14]

Temperature sensors operate through the process of converting thermal stimuli into electrical signals and measuring the response in terms of the resistance (*R*), voltage, or capacitance (*C*).[15-18] Someya et al. reported an R-based temperature sensor using a semi-crystalline acrylate polymer that demonstrated an excellent sensitivity of 0.02°C and a response time of 100 ms.[19] Bao et al. proposed decoupling the temperature and strain based on the temperature-sensitive relaxation time (τ) to provide a new solution for multimodal sensation.[20] Many studies have focused on improving the sensitivity and response time of temperature sensors. However, directly mimicking the various thermosensation functions of human skin remains a major challenge. Zhu et al. applied multimodal Pt film sensors to perceive wind and matter by using a heated Pt element to recognize contact with a cold object according to conductive heat transfer.[21] The heated Pt element could also recognize heat transfer from the wind at various flow angles (0°–90°) and flow rates (0–6 m s^{-1}). The pressure was sensed by covering the heated Pt element with a porous elastomer, whose thermal conductivity could be measured to detect elastic deformation induced by external stimuli. However, fully realizing all of the thermosensation functions of human skin remains a challenge, especially the recognition of heat sources. Heat source recognition is a critical function of the human skin, though its importance has not yet been fully identified. Humans can accurately recognize heat sources, determine their degree of heat exchange, and decide on the action, such as stepping away from strong sunlight into tree shade to avoid sunburning or going to a lakeside to enjoy the breeze to relax. Similarly, artificial limbs, or robots being furnished with heat source recognition, are capable of making precise determinations regarding multiple thermal stimuli in the environment without the assistance of other mechanical sensing, enabling them to carry out operations more rapidly and attain deeper and more intelligent bionics of the human body.

In this study, a heat source recognition sensor (*hsr* sensor) was developed to mimic the thermosensation function of human skin. The *hsr* sensor utilizes an ionic gel of poly(butyl acrylate)-lithium bis(n-fluoroalkylsulfonyl)imide (PBA-Li:*n*FSI; *n* = 1, 3, 5) in a capacitive structure with simultaneous temperature-, proximity-, and pressure-sensing functions. On the basis of the ionic relaxation behavior, the *hsr* sensor offers a high detection sensitivity of 0.005°C, a linear response over an ultra-wide temperature range (−20°C to 180°C), and excellent stability. The capacitive structure demonstrates a large positive change in *C* in response to external pressure, whereas a negative change in *C* is associated with a surface charge resulting from proximity to stimuli. We have systematically illustrated the heat source recognition function of the *hsr* sensor in various scenarios, such as radiation, convection, and conduction, by combining different combinations of sensing functions. We also showcased the integration of the *hsr* sensor with the isothermal regulation element to obtain multidimensional thermal information including the temperature, comfort level, and type of heat source. Our work presents a simple and direct solution for distinguishing the types of heat sources and opens up a new gateway for the field of e-skin.

RESULTS AND DISCUSSION

Concept of heat source recognition

Figure 1 shows the design concept of the proposed *hsr* sensor. Humans are surrounded by various heat sources in their environment (Figure 1A). The human skin is not only capable of feeling hot and cold but also recognizing the type of heat source (i.e., radiation, convection, and conduction) based on the difference between the environmental temperature and its own temperature. In heat exchange scenarios, heat sources and objects generate both physical and thermal stimuli.[22,23] External pressure provides additional information that allows the human skin to distinguish between different types of heat sources. Thermal radiation causes only temperature stimuli with no physical stimuli because of the absence of direct contact. Thermal convection results in both thermal and pressure stimuli because heat is exchanged by a fluid such as air. Finally, thermal conduction generates proximity, pressure, and thermal stimuli because it involves direct contact with a heat source. While the actual mechanism used by

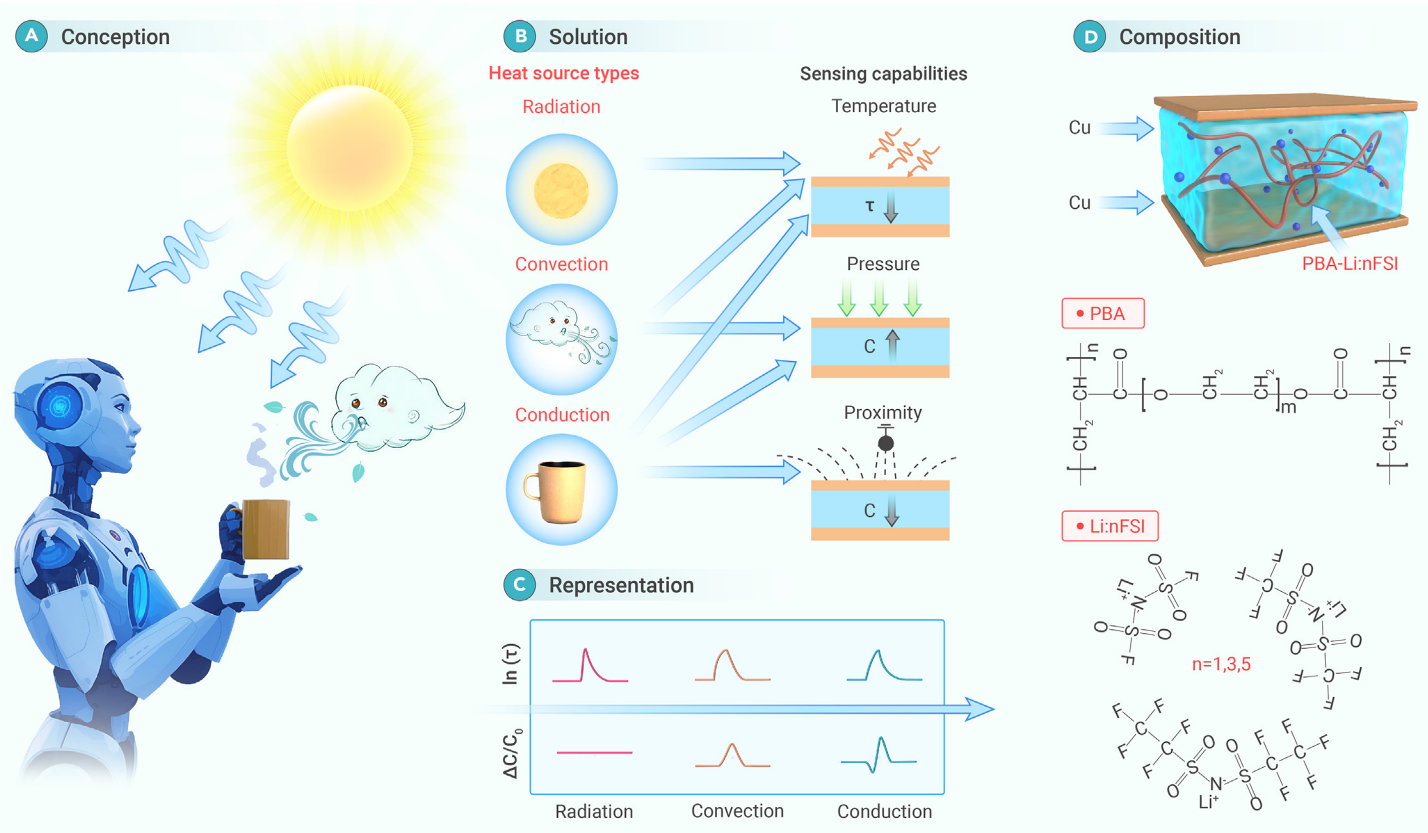

Figure 1. Design concept and application mechanism of the proposed *hsr* sensor by using the ionic relaxation dynamic behavior (A) Heat sources in the external environment. (B) Decomposition of heat source signals by *hsr* sensor. (C) Signal responses for different types of heat sources. (D) Structure and materials of the *hsr* sensor.

human skin to realize heat source recognition is outside the scope of this study, the differences between the heat transfer modes, as elucidated above, can be used to develop a *hsr* sensor that mimics its functions (Figure 1B).

The proposed *hsr* sensor is based on the relaxation behavior of an ionic gel, PBA-Li:*n*FSI (n = 1, 3, 5), which is placed in a capacitive structure with copper electrodes (Figure 1D). The ion relaxation time (τ) is an intrinsic parameter that only responds to variations in temperature, and it is unaffected by other signals, which makes it suitable for detecting thermal stimuli.[20] In contrast, the C can detect pressure stimuli,[24,25] and a negative change in C can be used to detect proximity stimuli.[26,27] Thus, a radiative heat source would only affect $ln(\tau)$, a convective heat source would affect $ln(\tau)$ and have only a positive $\Delta C/C_0$, and a conductive heat source would affect $ln(\tau)$ and have both a negative and positive $\Delta C/C_0$ (Figure 1C).

Ionic relaxation dynamic behavior of PBA-Li:*n*FSI

Figure 2 shows the relaxation behavior of the *hsr* sensor by using the ionic gel of PBA-Li:*n*FSI (n = 1, 3, 5). The frequency-dependent impedance of PBA-Li:5FSI can be characterized by Bode (Figure 2A) and Nyquist plots (Figure 2B). In the Bode plot, the high-frequency region is dominated by the imaginary impedance (Z_{im}) due to polarization, whereas the mid-frequency region is dominated by the real impedance (Z_{re}) due to ion migration. The equivalent circuit model was used to obtain the relaxation time τ (Figure S1; Text S1), which represents the time it takes for the polarization of the ions to vanish and is equal to the product of the bulk R and bulk C (i.e., $\tau = RC$).[20,28] R and C can be approximated by the Z_{re} ($R \approx Z_{re}$) in the flat region and the Z_{im} ($C \approx 1/\omega Z_{im}$) in the diagonal region, respectively. Charge relaxation occurs in the transition region between the middle and high frequencies, and the relaxation frequency (τ^{-1}) corresponds to the intersection between the Z_{re} (flat line) and the Z_{im} (diagonal line). In the Nyquist plot, the relaxation frequency corresponds to the position where the Z_{re} and Z_{im} are equal. An increase in temperature raises the relaxation frequency, but a change in pressure does not affect its value.

The signal response of the *hsr* sensor of PBA-Li:5FSI in the temperature range of −20°C to 180°C (Figure 2C) shows that as the temperature was increased, R decreased from 18.9 MΩ to 9.6 kΩ. This was ascribed to increased movement of polymer chains at higher temperatures, facilitating Li^+ ion transportation and increased conductivity. Meanwhile, C initially increased with the temperature and then decreased, reaching its maximum value at 20°C. The change in C was smaller than the change in R. The response of the *hsr* sensor based on the relaxation time ($\tau = RC$) (Figure 2D) showed a high level of linearity of 0.997 with temperature in the range of -20 to 180°C, with adecrease from −7.82 at −20°C to −17.03 at 180°C. These results show that the *hsr* sensor had a detection range of more than 200°C, much greater than other ionic gels in the literature (Table S1).[20,29,30] The slope of $ln(\tau)$ versus 1,000/T can be used to measure the sensitivity of the relaxation time to the temperature. The slope of (τ) versus 1,000/T was compared for ionic gels according to the fluorine content (PBA-Li:*n*FSI [n = 1, 3, 5]) (Figures 2E and S2). F–S bonds are less stable and heat resistant than C–S and C–C bonds. As the fluorine content increases, the number of C–S and C–C bonds increases, so the stability of lithium salts increases significantly. Increasing the fluorine content slightly decreased the measurement sensitivity but greatly increased the detection range, which indicates an inverse relationship between the sensitivity and range.

The measurement accuracy of the *hsr* sensor was evaluated according to the response of the relaxation time to changes in temperature (Figures 2F and S3). As τ is proportional to 1,000/T while not to T, the measurement accuracy of *hsr* sensors decreases with increasing ambient temperature. At room temperature, the relaxation time showed a noticeable response when the heat source temperature increased from 25°C by only 0.005°C. Thus, the *hsr* sensor demonstrated exceptional sensitivity to small fluctuations in temperature of 0.005°C, which exceeds that of many temperature sensors (Table S2).[31-33] We also investigated the effect of different thicknesses of ion gel films (PBA-Li:5FSI) on the accuracy of temperature measurement. We found that as the thickness of the ion gel film increases, the signal noise of the *hsr* sensor also increases, thus reducing the performance of the *hsr* sensor (Figure S4). The response time was only 200 ms (Figure 2G), which confirms that the *hsr* sensor can be applied to real-time temperature measurement. The real-time signal output was consistent and uniform throughout 50 temperature cycles with $ln(\tau)$ values ranging from −10.79 to −11.22 (Figures 2H and S3).

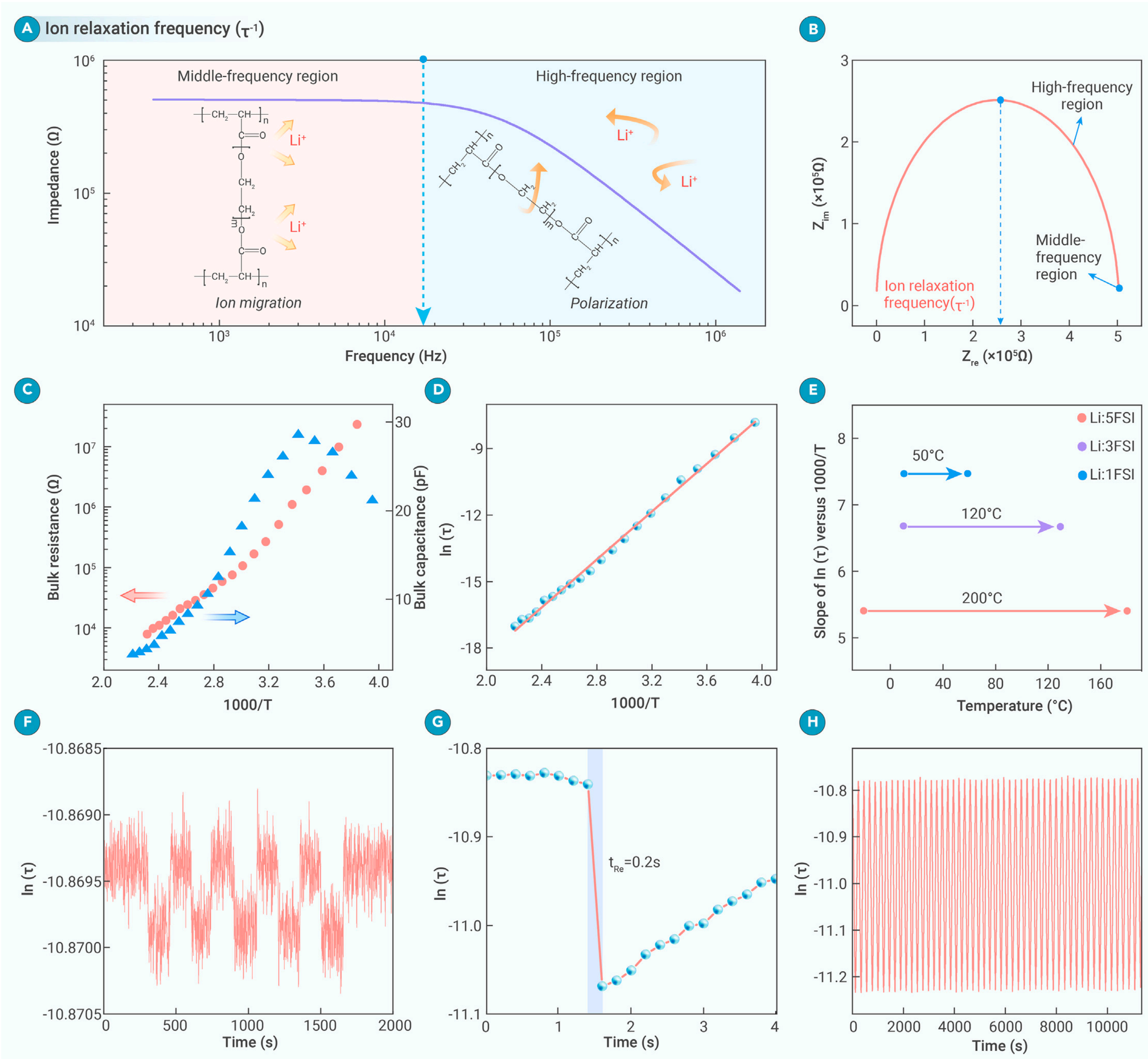

Figure 2. Ionic relaxation dynamic behavior of the *hsr* sensor by using the ionic gel of PBA-Li:*n*FSI (*n* = 1, 3, 5) (A and B) Bode plot (A) and Nyquist plot (B) of PBA-Li:5FSI gel at 30°C. (C) Bulk resistance and bulk capacitance responses in the temperature range of −20°C to 180°C. (D) Linear response of relaxation time in the temperature range of −20°C to 180°C (PBA-Li:5FSI gel). (E) Slope of (τ) versus 1,000/T according to the fluorine content (PBA-Li:*n*FSI [*n* = 1, 3, 5]). (F) Measurement accuracy for sensor with PBA-Li:5FSI gel film thickness of 100 μm at 25°C with a temperature change of 0.005°C. (G) Response time. (H) Stability over multiple temperature cycles (PBA-Li:5FSI gel).

Multidimensional sensing performance

Figure 3 explores the multidimensional sensing performance of the PBA-Li:5FSI-based *hsr* sensor under complicated thermal and pressure stimuli. Under pressure-free conditions, the temperature-dependent Bode plot (Figure 3A) shows that the impedance decreased from 1.73 MΩ at low frequencies to 211 kΩ at 1 kHz. In contrast, the relaxation frequency increased as the temperature increased from 15°C to 45°C. These results may be because a high temperature reduces the active energy for ionic migration, decreasing impedance at low frequencies. On the other hand, the dielectric coefficient is less sensitive to changes in temperature than the conductivity. Therefore, the change in *C* is small, so the relaxation frequency increases with the temperature.[34]

When the pressure was changed while the temperature was kept constant, the impedance spectrum shifted downwards (Figure 3B). The impedance decreased from 1.57 to 1.16 MΩ at 1 kHz, while the relaxation frequency (τ^{-1}) remained constant at 2.4 kHz. Increasing the pressure caused the *hsr* sensor to decrease in thickness and increase in area. Thus, *R* decreased at the mid-frequency region, and *C* increased for the high-frequency region. Therefore, τ^{-1} remained unchanged at different pressures because the change in *R* offset the change in C.[20] When both the temperature (20°C–50°C) and pressure (0–20 kPa) were varied, the curve of τ versus 1,000/*T* showed a good linear correlation with the temperature but was insensitive to changes in pressure (Figure 3C). In other words, the relaxation time response is ideal for measuring the temperature in environments with complicated thermal and pressure stimuli.

The *C* is influenced by the dimensions of the sensing region or volume, and it can be used to monitor changes in dimensions (Figure S5). In contrast, the relaxation time τ is not affected by compensation effects due to pressure. To eliminate the influence of temperature, the normalized *C* (i.e. $\Delta C/C_0$) can be determined from τ. $\Delta C/C_0$ varies linearly with the pressure, and it is insensitive to temperature changes (Figure 3D). Thus, it can be used to measure the pressure independent of changes in temperature. The *hsr* sensor demonstrated an excellent

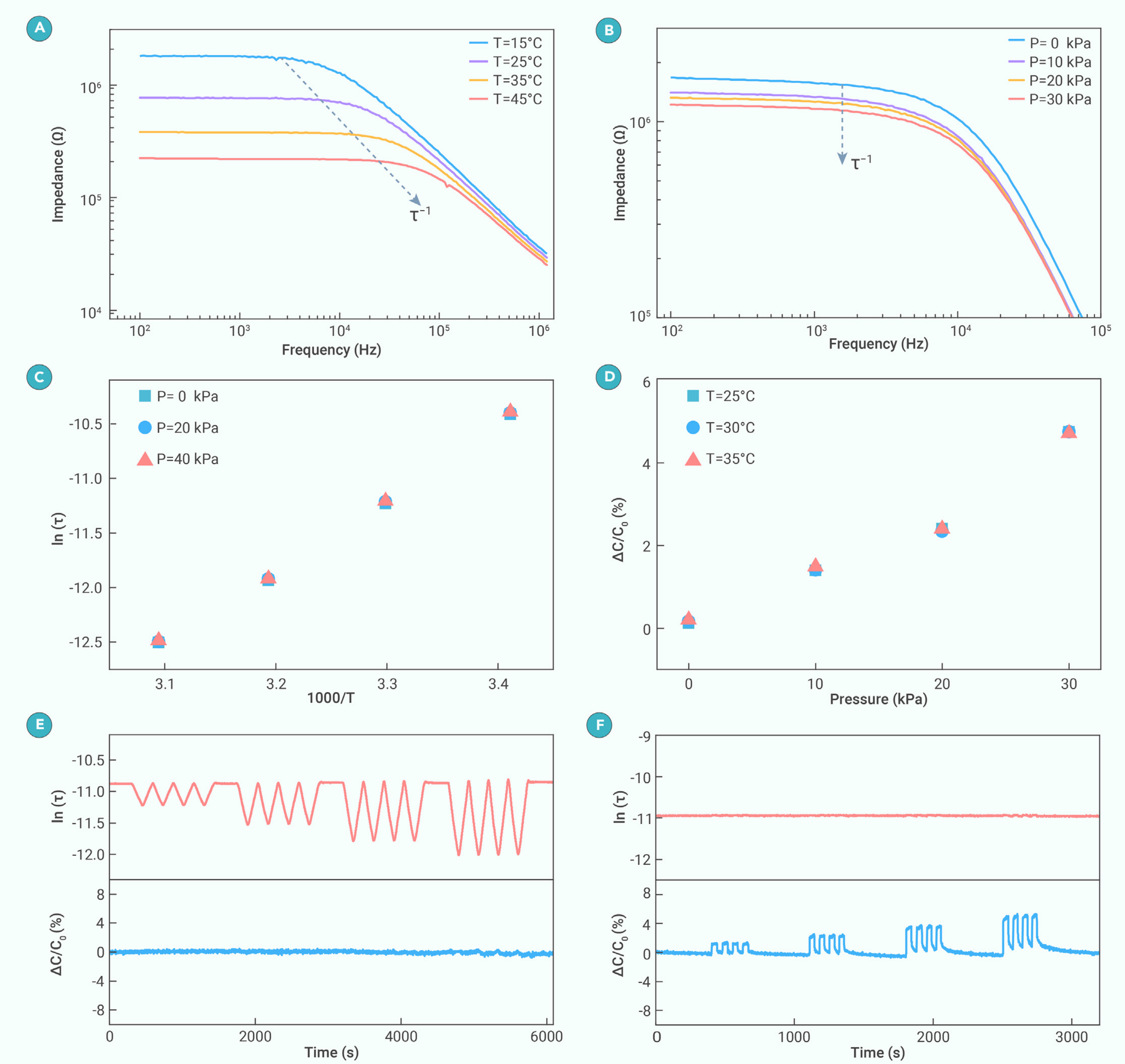

Figure 3. Signal decoupling mechanism for the PBA-Li:5FSI-based *hsr* sensor (A and B) Bode plots at different (A) temperatures and (B) pressures. (C) Response of $ln(\tau)$ to thermal and pressure stimuli. (D) Response of $\Delta C/C_0$ to different thermal and pressure stimuli. (E) Signal response to thermal stimuli. (F) Signal response to pressure stimuli.

pressure-sensing capability, and it could detect pressure stimuli as little as 100 Pa (Figure S5).

Increasing the temperature of the heat source from 25°C to 45°C (Figures 3E and S5) caused $ln(\tau)$ to decrease from -10.88 to -11.53 consistently. $\Delta C/C_0$ remained at zero in the absence of any pressure stimuli, and it was unaffected by changes in temperature. Increasing the pressure from 0 to 10 kPa (Figures 3F and S7) caused $\Delta C/C_0$ to increase from 0 to 1.49% across multiple tests. Increasing the pressure to 40 kPa caused $\Delta C/C_0$ to reach 5.21%. In contrast, τ remained around 10.93 at different pressures. This complete decoupling between the temperature and pressure responses demonstrates the potential of the PBA-Li:5FSI-based *hsr* sensor for multimodal sensing.

Moreover, the PBA-Li:5FSI-based *hsr* sensor also showed proximity sensing. When an object approaches the top electrode, it induces a charge in the conductor and electrode, redistributing the electric field and causing a negative change in the C (Figure S7). The magnitude of the induced charge depends on the charge of the conductor, distance of the object, and speed of the object. Bringing a finger within 1 cm of the *hsr* sensor affected the electric field of the parallel plate capacitor and changed $\Delta C/C_0$ by approximately -0.4%.

Heat source recognition function

The human skin facilitates the body's interaction with the external environment and enables the detection of various stimuli such as heat, touch, and pain.[35] The unique response mechanisms of the proposed *hsr* sensor to changes in temperature, pressure, and proximity can be used to distinguish between different types of heat transfer: conduction, convection, and radiation. Here, we show the concept proving of the heat source recognition function by using the as-fabricated PBA-Li:5FSI-based *hsr* sensor.

For a radiative heat source, the *hsr* sensor relies on measuring variations in temperature without any changes in external force or electrical charge

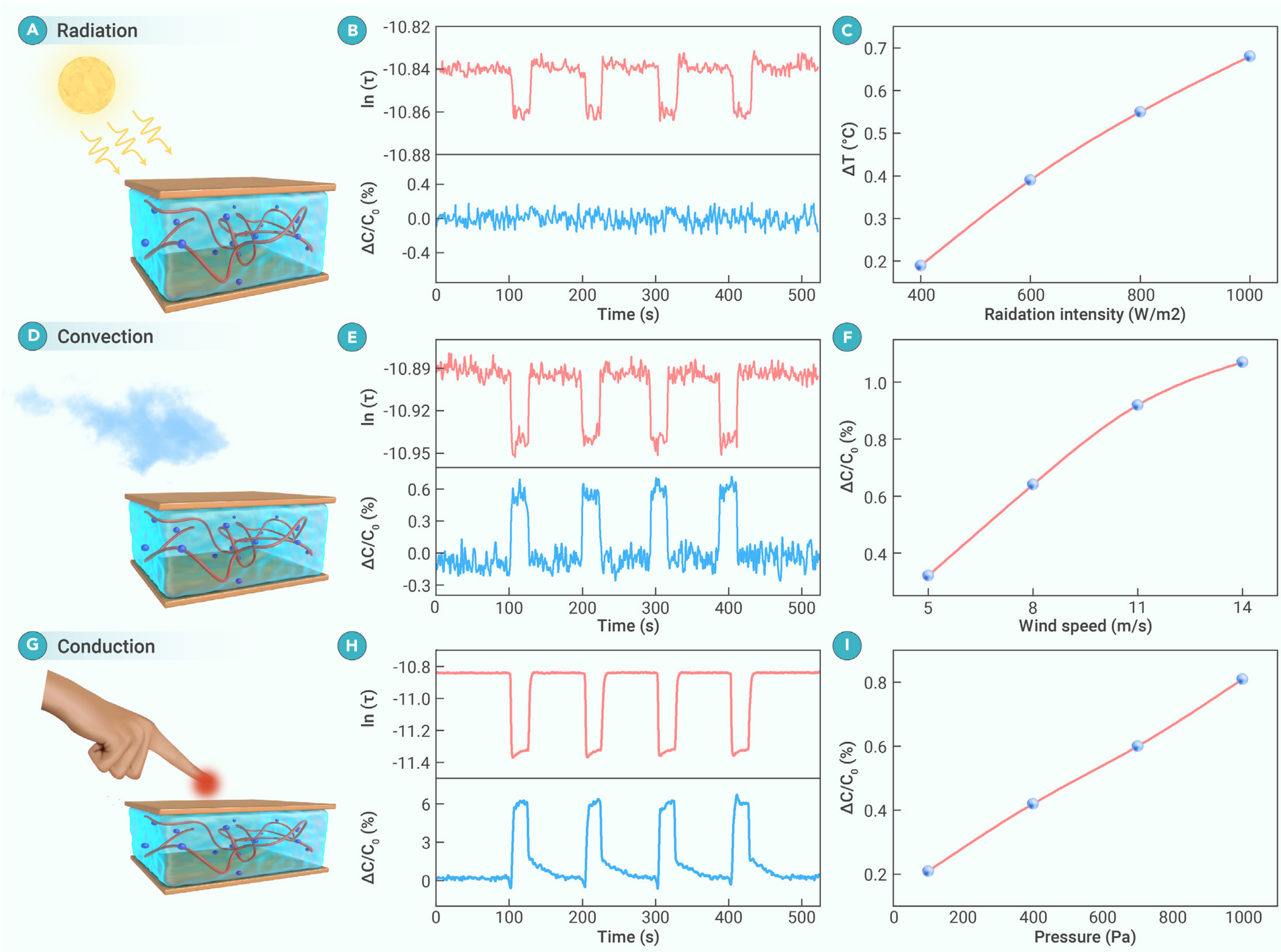

Figure 4. Heat source recognition function of the proposed PBA-Li:5FSI-based *hsr* sensor (A) Detection of a radiative heat source. (B) (τ) and $\Delta C/C_0$ at a radiation intensity of 600 W/m^2. (C) ΔT at different radiation intensities. (D) Detection of a convective heat source. (E) (τ) and $\Delta C/C_0$ for an airflow with a temperature of 25°C and speed of 11 m/s. (F) $\Delta C/C_0$ at different airflow speeds. (G) Detection of a conductive heat source. (H) (τ) and $\Delta C/C_0$ when subjected to pressure from a finger at a temperature of 34°C. (I) $\Delta C/C_0$ at different pressures.

(Figure 4A). Under four radiation stimuli comprising simulated sunlight with a light intensity of 600 W/m^2 and a duration of 5 s (Figure 4B), each stimulus caused τ to decrease from −10.84 to −10.86, which corresponded to an increase in temperature of 0.38°C. In contrast, $\Delta C/C_0$ remained constant. These consistent responses of τ and $\Delta C/C_0$ show that the *hsr* sensor is capable of detecting and recognizing radiative heat sources. Next, stimuli of different radiation intensities were tested (Figure 4C). A radiation intensity of 400 W/m^2 increased the temperature measured by the *hsr* sensor by approximately 0.19°C, and a radiation intensity of 1,000 W/m^2 increased the temperature by 0.68°C. Thus, the radiation intensity of the radiative heat source can be determined based on changes in the measured temperature.

Thermal convection affects both the temperature and capacitance of the *hsr* sensor due to the pressure exerted by an airflow on its surface. Under a thermal stimulation of a convective heat source, the *hsr* sensor generates both the variations in τ and $\Delta C/C_0$ caused by thermal and pressure stimuli (Figure 4D). Applying an airflow at a temperature of 25°C and a speed of 11 m/s for 5 s (Figure 4E) shifted τ from −10.89 to −10.95, which corresponded to a rapid temperature increase of approximately 0.98°C. At the same time, $\Delta C/C_0$ shifted approximately 0.64%, which distinguished the convective heat source from a radiative heat source. A positive correlation was identified between the magnitude of the change in C and the airflow speed (Figure 4F). Specifically, $\Delta C/C_0$ was 0.21% at an airflow speed of 5 m/s and increased to 0.92% at an airflow speed of 14 m/s.

Finally, for a conductive heat source (Figure 4G), the proposed *hsr* sensor feeds back an initial negative change and then a positive change in $\Delta C/C_0$, corresponding to the source approaching and touching the sensor. Meanwhile, the change in (τ) can be used to measure the temperature of the heat source. When a finger at 34°C approached and then touched the *hsr* sensor (Figure 4H), $\Delta C/C_0$ was observed to first decrease by −1% and then increase by 6.2%, while *ln*(τ) decreased from −10.84 to −11.3. The initial negative *C* distinguishes thermal conduction from thermal convection. As the finger approached the sensor before contact, the charge in the surface electric field generated a *C* signal that can be used to detect the proximity of the heat source. This change in *C* opposes the effect of external pressure, which makes it easy to distinguish between conductive and convective sources. The changes in $\Delta C/C_0$ at different pressure intensities (Figure 4I) demonstrate that the ionic gel deformed more as the pressure increased, increasing the *C*.

The human-like thermosensation function

We combined the PBA-Li:5FSI-based *hsr* sensor with an e-skin with isothermal regulation to mimic human-like thermosensation capabilities. The e-skin is comprised of a flexible thermoelectric device and a flexible heat sink made from phase-change materials, as described in previous works.[4,5] The e-skin was laminated on a prosthesis, and the *hsr* sensor was attached to the surface (Figure 5A). The integrated system was finally attached to a robot to sense the temperature, comfort level, and type of heat source. The temperature was obtained from the correlation with τ. Meanwhile, previous studies have shown that a comfort temperature zone exists for the human body in scenarios with strong heat exchange.[36,37] The body feels cold if the temperature of the stimulus

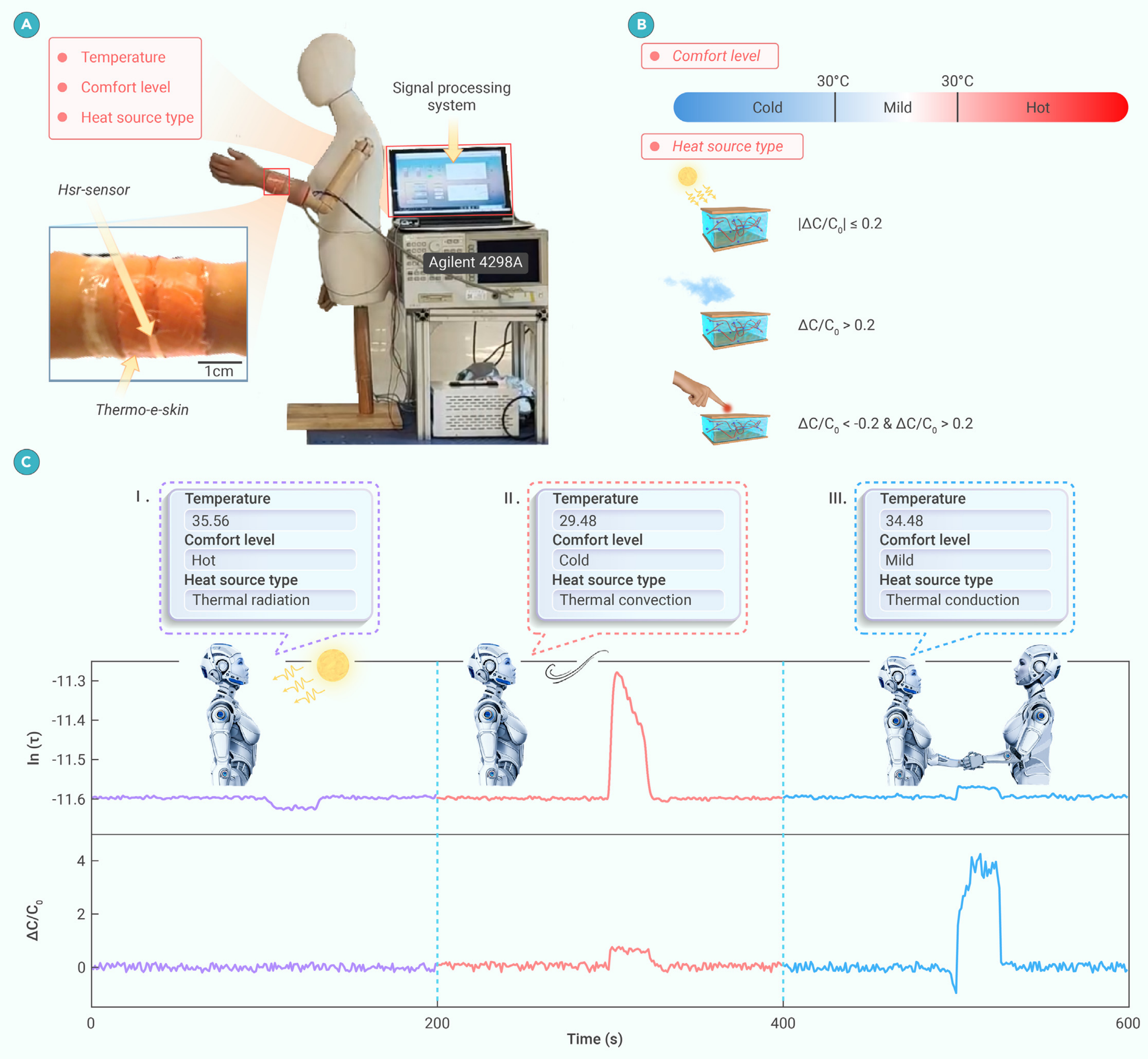

Figure 5. The robot integrated with a human-like thermosensation function (A) Establishment of the thermosensation system for the robot. (B) Schematic of the thermosensation system. (C) The thermosensation of robot in different scenarios.

is below 30°C, mild if the temperature of the stimulus is between 30°C and 35°C, and hot if the temperature of the stimulus is higher than 35°C. Therefore, the physical comfort level of the heat source in strong heat exchange scenarios could be determined from the measured temperature. Finally, the different signal responses of the *hsr* sensor could be used to recognize the type of heat source. Heat sources were classified as radiative if $|\Delta C/C_0| \leq 0.2$, convective if $\Delta C/C_0 > 0.2$, and conductive if $\Delta C/C_0 < 0.2$ and $\Delta C/C_0 > 0.2$ (Figure 5B).

The effectiveness of the thermosensation system was verified in experiments where the robot was exposed to different stimuli while the surface temperature of the prosthesis was maintained at 35°C. Three scenarios were considered (Figure 5C; Video S1): (1) the robot was exposed to sunlight outdoors, (2) the robot moved indoors and was subjected to airflow, and (3) the robot shook hands with another robot indoors.

In scenario 1, the robot was exposed to sunlight. The heat from the sunlight affects the surface temperature of the robot through radiation. At this time, the *hsr* sensor detects the temperature stimulus and transmits the signal to the signal processing system. The robot can then determine a temperature value of 35.56°C, with a body sensation of hot, and the heat source type was thermal radiation. In scenario 2, the robot was in a convective environment by facing a hair dryer. The robot relied on the *hsr* sensor and the signal processing system to determine the temperature value as 29.48°C, with a body sensation of cold, and the heat source type was thermal convection. In scenario 3, the robot shook hands with a human, which involved the direct transfer of heat. According to the τ and $\Delta C/C_0$ values of the *hsr* sensor, the robot was simultaneously subjected to temperature stimulus, proximity stimulus, and pressure stimulus and determined the temperature to be 34.48°C, with a mild body sensation, and the type of heat source was thermal conduction. Our work provides insight into the thermal function of e-skin. The proposed heat source recognition would have a significant impact on the e-skin field, especially for the highly environment-sensitive robots and the thermosensation rebuilding of prosthetics.

CONCLUSION

In this study, an *hsr* sensor was developed that uses the relaxation behavior of ionic gels (PBA-Li:*n*FSI, $n = 1, 3, 5$) to distinguish between different types of heat sources. The *hsr* sensor has a multimodal response to heat, pressure, and proximity. It shows a high sensitivity of 0.005°C and a wide measurement range of −20°C to 180°C based on the changes in τ. It also has high sensitivity and a quick response time to pressure (positive $\Delta C/C_0$) and proximity (negative $\Delta C/C_0$) stimuli. The distinguishing of radiative, convective, and conductive heat sources was realized by combinations of the τ and $\Delta C/C_0$ responses to external stimuli. In experiments, the *hsr* sensor reliably distinguishes different types of heat sources at different intensities. The *hsr* sensor was then combined with an e-skin with isothermal regulation and attached to a robot to mimic a human-like thermosensation function. This study provides insight into the thermosensation capabilities of e-skin. The proposed *hsr* sensor would significantly impact the e-skin field, especially regarding the development of environment-sensitive robots and prosthetics with thermosensation function.

MATERIALS AND METHODS

See the supplemental information for details.

REFERENCES

1. Guyton, A.C., and Hall, J.E. (1986). Textbook of Medical Physiology (Saunders).
2. Kurz, A. (2008). Physiology of thermoregulation. Best Pract. Res. Clin. Anaesthesiol. ***22***(4): 627–644. https://doi.org/10.1016/j.bpa.2008.06.004.
3. Terrien, J., Perret, M., and Aujard, F. (2011). Behavioral thermoregulation in mammals: a review. Front. Biosci. ***16***(4): 1428–1444. https://doi.org/10.2741/3797.
4. Zhang, P., Deng, B., Zhu, K., et al. (2022). Wide-temperature range thermoregulating e-skin design through a hybrid structure of flexible thermoelectric devices and phase change materials heat sink. EcoMat ***4***(6): e12253. https://doi.org/10.1002/eom2.12253.
5. Zhang, P., Li, Z., Wang, Y., et al. (2024). Electronic skin with biomimetic structures realizes excellent isothermal regulation. Nano Energy ***121***: 109189. https://doi.org/10.1016/j.nanoen.2023.109189.
6. Gong, S., Wang, Y., Yap, L.W., et al. (2018). A location-and sharpness-specific tactile electronic skin based on staircase-like nanowire patches. Nanoscale Horiz. ***3***(6): 640–647. https://doi.org/10.1039/C8NH00125A.
7. Wang, Y., Gong, S., Wang, S.J., et al. (2016). Volume-invariant ionic liquid microbands as highly durable wearable biomedical sensors. Mater. Horiz. ***3***(3): 208–213. https://doi.org/10.1039/C5MH00284B.
8. Deng, S., Li, Y., Li, S., et al. (2024). A multifunctional flexible sensor based on PI-MXene/SrTiO3 hybrid aerogel for tactile perception. Innovation ***5***(3): 100596. https://doi.org/10.1016/j.xinn.2024.100596.
9. Patapoutian, A., Peier, A.M., Story, G.M., et al. (2003). Thermotrp channels and beyond: Mechanisms of temperature sensation. Nat. Rev. Neurosci. ***4***(7): 529–539. https://doi.org/10.1038/nrn1141.
10. Vriens, J., Nilius, B., and Voets, T. (2014). Peripheral thermosensation in mammals. Nat. Rev. Neurosci. ***15***(9): 573–589. https://doi.org/10.1038/nrn3784.
11. Cabanac, M. (1975). Temperature regulation. Annu. Rev. Physiol. ***37***(1): 415–439. https://doi.org/10.1146/annurev.ph.37.030175.002215.
12. Hensel, H., and Schafer, K. (1984). Thermoreception and Temperature Regulation in Man (Springer).
13. Chortos, A., Liu, J., and Bao, Z.A. (2016). Pursuing prosthetic electronic skin. Nat. Mater. ***15***(9): 937–950. https://doi.org/10.1038/nmat4671.
14. Yu, X.G., Xie, Z.Q., Yu, Y., et al. (2019). Skin-integrated wireless haptic interfaces for virtual and augmented reality. Nature ***575***(7783): 473–479. https://doi.org/10.1038/s41586-019-1687-0.
15. Jeon, J., Lee, H.B.R., and Bao, Z. (2013). Flexible wireless temperature sensors based on Ni microparticle-filled binary polymer composites. Adv. Mater. ***25***(6): 850–855. https://doi.org/10.1002/adma.201204082.
16. Park, T.H., Park, S., Yu, S., et al. (2021). Highly sensitive on-skin temperature sensors based on biocompatible hydrogels with thermoresponsive transparency and resistivity. Adv. Healthcare Mater. ***10***(14): 2100469. https://doi.org/10.1002/adhm.202100469.
17. Ren, X.C., Pei, K., Peng, B.Y., et al. (2016). A low-operating-power and flexible active-matrix organic-transistor temperature-sensor array. Adv. Mater. ***28***(24): 4832–4838. https://doi.org/10.1002/adma.201600040.
18. Yu, Y., Guo, J., Zhang, H., et al. (2022). Shear-flow-induced graphene coating microfibers from microfluidic spinning. Innovation ***3***(2): 100209. https://doi.org/10.1016/j.xinn.2022.100209.
19. Yokota, T., Inoue, Y., Terakawa, Y., et al. (2015). Ultraflexible, large-area, physiological temperature sensors for multipoint measurements. Proc. Natl. Acad. Sci. USA ***112***(47): 14533–14538. https://doi.org/10.1073/pnas.1515650112.
20. You, I., Mackanic, D.G., Matsuhisa, N., et al. (2020). Artificial multimodal receptors based on ion relaxation dynamics. Science ***370***(6519): 961–965. https://doi.org/10.1126/science.aba5132.
21. Zhao, S., and Zhu, R. (2017). Electronic skin with multifunction sensors based on thermosensation. Adv. Mater. ***29***(15): 1606151. https://doi.org/10.1002/adma.201606151.
22. Huang, Y., Zhou, J., Ke, P., et al. (2023). A skin-integrated multimodal haptic interface for immersive tactile feedback. Nat. Electron. ***6***: 1020–1031. https://doi.org/10.1038/s41928-023-01074-z.
23. Zhao, H., Zhang, Y., Han, L., et al. (2023). Intelligent Recognition Using Ultralight Multifunctional Nano-Layered Carbon Aerogel Sensors with Human-Like Tactile Perception. Nano-Micro Lett. ***16***(1): 11. https://doi.org/10.1007/s40820-023-01216-0.
24. Bai, N.N., Wang, L., Wang, Q., et al. (2020). Graded intrafillable architecture-based iontronic pressure sensor with ultra-broad-range high sensitivity. Nat. Commun. ***11***(1): 209. https://doi.org/10.1038/s41467-019-14054-9.
25. Gong, S., Schwalb, W., Wang, Y.W., et al. (2014). A wearable and highly sensitive pressure sensor with ultrathin gold nanowires. Nat. Commun. ***5***: 3132. https://doi.org/10.1038/ncomms4132.
26. Wang, H.T., Tang, Q.X., Zhao, X.L., et al. (2018). Ultrasensitive flexible proximity sensor based on organic crystal for location detection. ACS Appl. Mater. Interfaces ***10***(3): 2785–2792. https://doi.org/10.1021/acsami.7b15352.
27. Sarwar, M.S., Dobashi, Y., Preston, C., et al. (2017). Bend, stretch, and touch: Locating a finger on an actively deformed transparent sensor array. Sci. Adv. ***3***(3): e1602200. https://doi.org/10.1126/sciadv.1602200.
28. Haus, H.A., and Melcher, J.R. (1989). Electromagnetic Fields and Energy (Prentice Hall Englewood Cliffs).
29. Choi, H., and Jeong, U. (2023). Purposive design of stretchable composite electrodes for strain-negative, strain-neutral, and strain-positive ionic sensors. Adv. Mater. ***35***(52): 2306795. https://doi.org/10.1002/adma.202306795.
30. Kim, H.W., Kim, E., Oh, J., et al. (2022). Water-saturated ion gel for humidity-independent high precision epidermal ionic temperature sensor. Adv. Sci. ***9***(16): 2200687. https://doi.org/10.1002/advs.202200687.
31. Li, F., Xue, H., Lin, X.Z., et al. (2022). Wearable temperature sensor with high resolution for skin temperature monitoring. ACS Appl. Mater. Interfaces ***14***(38): 43844–43852. https://doi.org/10.1021/acsami.2c15687.
32. Li, L.T., Zhu, G.X., Wang, J., et al. (2023). A flexible and ultrasensitive interfacial iontronic multisensory sensor with an array of unique "cup-shaped" microcolumns for detecting pressure and temperature. Nano Energy ***105***: 108012. https://doi.org/10.1016/j.nanoen.2022.108012.
33. Seo, B., Hwang, H., Kang, S., et al. (2018). Flexible-detachable dual-output sensors of fluid temperature and dynamics based on structural design of thermoelectric materials. Nano Energy ***50***: 733–743. https://doi.org/10.1016/j.nanoen.2018.06.027.
34. Shim, Y., and Kim, H.J. (2013). Dielectric relaxation and solvation dynamics in a room-temperature ionic liquid: temperature dependence. J. Phys. Chem. B ***117***(39): 11743–11752. https://doi.org/10.1021/jp406353j.
35. Lumpkin, E.A., and Caterina, M.J. (2007). Mechanisms of sensory transduction in the skin. Nature ***445***(7130): 858–865. https://doi.org/10.1038/nature05662.
36. Gagge, A.P., Stolwijk, J., and Hardy, J.J.E.r. (1967). Comfort and thermal sensations and associated physiological responses at various ambient temperatures. Environ. Res. ***1***(1): 1–20. https://doi.org/10.1016/0013-9351(67)90002-3.
37. Kingma, B.R., Frijns, A.J., Schellen, L., et al. (2014). Beyond the classic thermoneutral zone: including thermal comfort. Temperature ***1***(2): 142–149. https://doi.org/10.4161/temp.29702.

ACKNOWLEDGMENTS

The authors acknowledge the financial support from the ShenZhen Innovation Program for Distinguished Young Scholars (RCJC20210706091949018), the Guangdong Provincial Key Laboratory Program (2021B1212040001) from the Department of Science and Technology of Guangdong Province, Tencent Foundation through the XPLORER PRIZE, The Hong Kong Polytechnic University (Project ZVQM), and the RGC Senior Research Fellow Scheme (SRFS2122-5S04).

AUTHOR CONTRIBUTIONS

All authors have contributed significantly to this work. W.S., P.Z., and W.L. conceived the idea; P.Z., W.S., X.L., Y.W., B.Y., and W.S. designed the experiments and performed the measurements; P.Z. and W.L. wrote the manuscript; Z.Z. provided valuable suggestions; and W.L. supervised the whole project.

DECLARATION OF INTERESTS

The authors declare no competing interests.

LEAD CONTACT WEBSITE

https://www.polyu.edu.hk/researchgrp/zzheng/
https://faculty.sustech.edu.cn/?tagid=liuws&iscss=1&snapid=1&orderby=date&go=1.

SUPPLEMENTAL INFORMATION

It can be found online at https://doi.org/10.1016/j.xinn.2024.100673.